molecular pharmaceutics

ARTICLE

pubs.acs.org/molecularpharmaceutics

A Mechanistic Study of Tumor-Targeted Corrole Toxicity

Jae Youn Hwang,[†] Jay Lubow,[†] David Chu,[†] Jun Ma,[†] Hasmik Agadjanian,[†] Jessica Sims,[†] Harry B. Gray,[‡] Zeev Gross,[§] Daniel L. Farkas,[†,‡,∥,⊥] and Lali K. Medina-Kauwe[*,†,#]

[†]Department of Biomedical Sciences and [∥]Department of Surgery, Cedars-Sinai Medical Center, Los Angeles, California, United States

[‡]Beckman Institute, California Institute of Technology, Pasadena, California, United States

[§]Schulich Faculty of Chemistry, Technion—Israel Institute of Technology, Haifa, Israel

[⊥]Department of Biomedical Engineering, University of Southern California, Los Angeles, California, United States

[#]Geffen School of Medicine, The University of California Los Angeles, Los Angeles, California, United States

Supporting Information

ABSTRACT: HerGa is a self-assembled tumor-targeted particle that bears both tumor detection and elimination activities in a single, two-component complex (Agadjanian et al. *Proc. Natl. Acad. Sci. U.S.A.* **2009**, *106*, 6105−6110). Given its multifunctionality, HerGa (composed of the fluorescent cytotoxic corrole macrocycle, S2Ga, noncovalently bound to the tumor-targeted cell penetration protein, HerPBK10) has the potential for high clinical impact, but its mechanism of cell killing remains to be elucidated, and hence is the focus of the present study. Here we show that HerGa requires HerPBK10-mediated cell entry to induce toxicity. HerGa (but not HerPBK10 or S2Ga alone) induced mitochondrial membrane potential disruption and superoxide elevation, which were both prevented by endosomolytic-deficient mutants, indicating that cytosolic exposure is necessary for corrole-mediated cell death. A novel property discovered here is that corrole fluorescence lifetime acts as a pH indicator, broadcasting the intracellular microenvironmental pH during uptake in live cells. This feature in combination with two-photon imaging shows that HerGa undergoes early endosome escape during uptake, avoiding compartments of pH < 6.5. Cytoskeletal disruption accompanied HerGa-mediated mitochondrial changes whereas oxygen scavenging reduced both events. Paclitaxel treatment indicated that HerGa uptake requires dynamic microtubules. Unexpectedly, low pH is insufficient to induce release of the corrole from HerPBK10. Altogether, these studies identify a mechanistic pathway in which early endosomal escape enables HerGa-induced superoxide generation leading to cytoskeletal and mitochondrial damage, thus triggering downstream cell death.

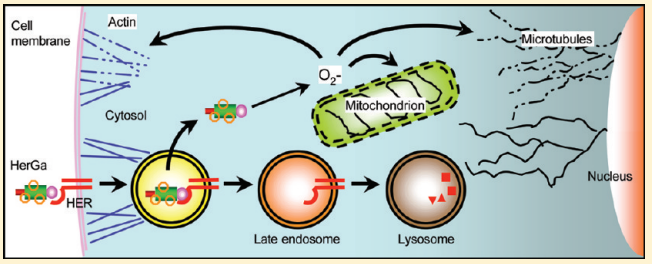

KEYWORDS: superoxide, mitochondria, cytoskeleton, tumor, targeting, gallium, corrole, heregulin, mechanism, HerGa

INTRODUCTION

Whereas cancer treatment by porphyrins and related macrocyclic compounds has been investigated extensively for many decades,[1,2] the therapeutic potential of corroles has only recently been disclosed.[3,4] Sulfonated corroles are water-soluble (amphipolar) macrocyclic compounds, whose Fe(III) and Mn(III) complexes are very active catalysts for decomposition of reactive oxygen and nitrogen species involved in a variety of relevant diseases.[5−9] Also noteworthy is the finding that Ga(III) and Al(III) derivatives are intensely fluorescent at relatively long wavelengths.[10,11] While these metal complexes are capable of undergoing endocytosis via co-uptake with, or noncovalent attachment to, serum proteins *in vitro* and *in vivo*, they are unable to penetrate cell membranes without facilitation by membrane-lytic molecules. Hence, toxic corroles, such as the Ga(III) derivative, are safe at pharmacologic doses but can kill cells when allowed to breach into the cytosol.[12]

Our investigations of S2Ga, the Ga(III) −metalated derivative of the sulfonated corrole, have shown that it noncovalently attaches to the ligand-directed cell penetration protein HerPBK-10 with sufficient stability as to not exchange with serum proteins.[3,12] We have further shown that HerGa (resulting from the noncovalent assembly of S2Ga and HerPBK10) can selectively target and kill HER2+ tumor cells in a mixed culture of HER2+ and HER2− cells[3] at submicromolar concentrations while the individual components comprising HerGa do not elicit cell death.[3,12]

Cell targeting by HerPBK10 is directed by the incorporation of the receptor-binding domain of heregulin, which has enhanced affinity for the human epidermal growth factor receptor (HER) heterodimer (HER2/3 or HER2/4) when the HER-2 subunit is amplified, such as in HER2+ tumors.[13,14] These tumors comprise the most aggressive and recalcitrant cancers with the worst prognosis among breast, prostate, and glioma tumors,[15−19] thus patients could benefit from targeted interventions. Current targeted therapies aimed at blocking proliferative signaling are

Received: February 25, 2011
Accepted: October 9, 2011
Revised: July 19, 2011
Published: October 10, 2011

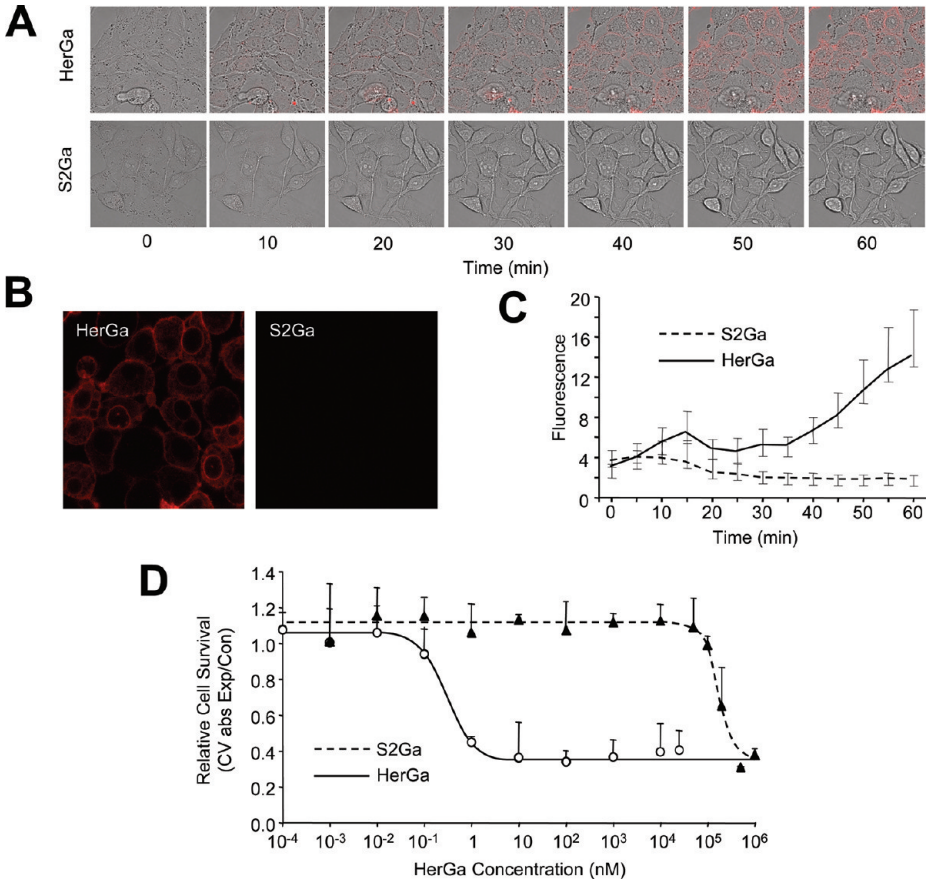

Figure 1. HerPBK10 is required for enhanced internalization and cell death. (A) MDA-MB-435 cells were exposed to either HerGa or S2Ga (1 μM final corrole concentration) and imaged live by fluorescence confocal microscopy. Micrographs show fluorescence and brightfield overlays at key time points of uptake. (B) Comparison of fluorescence images acquired at 1 h after HerGa or S2Ga uptake. (C) Quantification of uptake in panel A. The cytosolic accumulation of fluorescence in each cell was quantified by selecting cytosolic regions and averaging fluorescence intensity using Image J. (D) Cell death dose curve. MDA-MB-435 cells were incubated with HerGa or S2Ga at the indicated doses for 24 h before cell survival was assayed by crystal violet (CV) stain. Cell survival is expressed as CV absorbance of each HerGa-treated sample normalized by mock (PBS) treated samples, or CV abs of experimental/control. Error bars represent 1 SD of triplicate treatments.

ineffective in up to 70% of cases likely due to signaling mutations accumulated in tumor cells,[20,21] hence alternative targeting strategies that circumvent signal inhibition (such as the direct delivery of toxic molecules into tumor cells) could provide needed improvements. Accordingly, HerPBK10 was designed to enter cells via HER binding and rapid ligation-triggered internalization, followed by endosomal penetration via the adenovirus-derived penton base domain engineered into the protein.[3,12,22] Importantly, the current monoclonal antibodies used clinically for targeted therapy of HER2+ tumors do not undergo receptor-mediated endocytosis or membrane penetration.

Our previous studies have shown that HerGa binds tumor cells through competitively inhibitable HER binding, and undergoes endocytosis after receptor binding.[12] We have also shown that the corrole (detected by virtue of its fluorescence) remains sequestered throughout the cytoplasm and excluded from the nucleus,[3,12] thus pointing to cytosolic rather than nuclear factors as the targets of corrole-mediated cytotoxicity in human breast cancer cells.[12] The relevance of these studies to *in vivo* systems was demonstrated in tumor-implanted mice, which showed that HerPBK10 enables corrole targeting and uptake into HER2+ tumors that can be readily visualized due to the intense corrole fluorescence, and this tumor targeting resulted in tumor growth inhibition at >5-times lower dosage in comparison to systemic delivery of the chemotherapy agent, doxorubicin.[3,4] These initial successes in testing corroles for tumor-targeted therapy have highlighted the need to elucidate the underlying mechanisms that contribute to corrole-mediated cytotoxicity.

The focus of this study is to examine the intracellular changes taking place after HerGa uptake that precede cell death, so as to delineate the events that cause HerGa-mediated toxicity. The present study shows that HerGa, but not HerPBK10 or S2Ga alone, compromises mitochondrial membrane potential [$\Delta\Psi$(m)] and disrupts the cytoskeleton through superoxide elevation, for which escape from endosomal vesicles after cell uptake is key. While low pH does not induce corrole release from the carrier, HerGa avoids highly acidic intracellular compartments, as assessed by fluorescence lifetime imaging and two-photon imaging and through the use of endosomolytic-defective versions of the carrier protein. Importantly, the fluorescence lifetime characteristics of the corrole enabled us to identify the intracellular compartmental pH of its surrounding microenvironment during cellular uptake, thus acting as a pH indicator in live cells. Studies with paclitaxel indicate that dynamic microtubules are required for HerGa uptake. These findings have allowed us to identify for the first time the intracellular events that facilitate HerGa

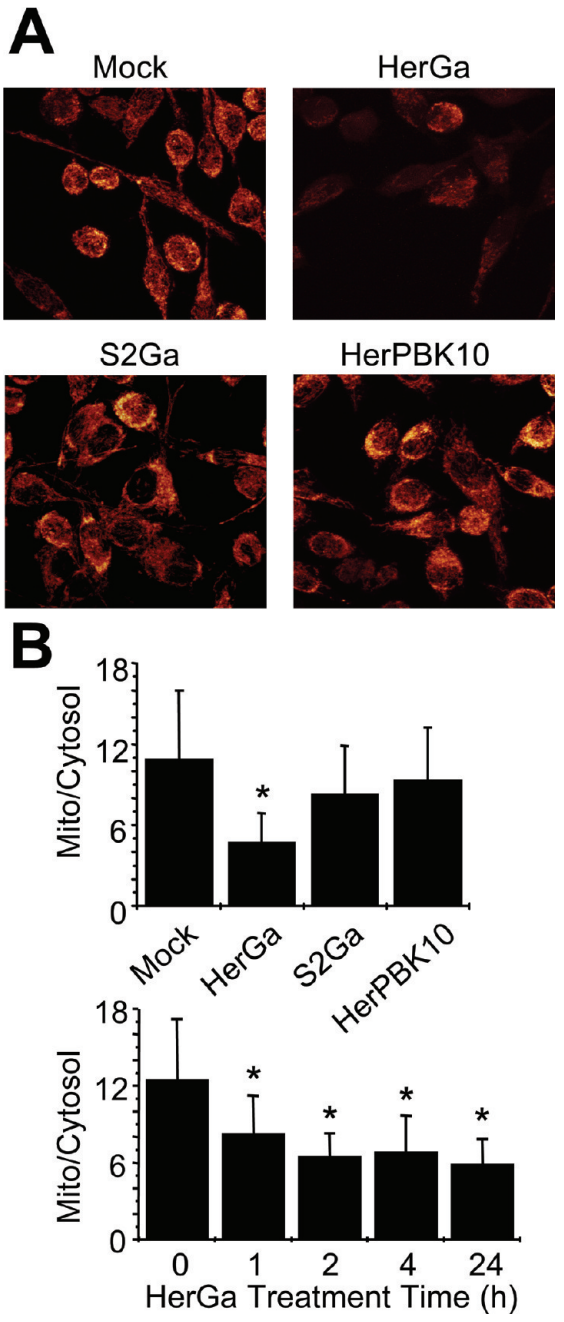

Figure 2. HerGa impacts mitochondrial membrane permeability. MDA-MB-435 cells exposed to HerGa or S2Ga (at 1 μM corrole concentration), HerPBK10, or PBS received 20 nM TMRM in PBS at 24 h after treatment, followed by two-photon excited confocal fluorescence imaging after TMRM uptake. (A) Cells displaying respective fluorescences as the *z*-stacked maximum intensity projection of each acquired fluorescence image. (B, upper) Mitochondria/cytoplasm ratio of TMRM fluorescence averaged from three independent experiments represented by panel A (TMRM uptake). For each experiment, the average fluorescence intensity for 10 different mitochondrial regions and that for one mitochondria-free region (cytoplasm) within the same cells were measured respectively. (B, lower) Time course of membrane collapse. TMRM uptake during HerGa treatment was assessed as described in the Materials and Methods with mitochondrial/cytoplasm TMRM fluorescence ratios obtained at the indicated time points after HerGa treatment. *, $P < 0.05$ compared to (B, upper) mock (PBS) treatment, or (B, lower) time point 0, as determined by 2-tailed unpaired *t* test.

interaction with target cells leading to corrole-mediated cytotoxicity, and may be applicable to a broad range of tumors depending on the delivery vehicle.

MATERIALS AND METHODS

Materials. HerPBK10, HerK10, and Her protein were produced in and isolated from a bacterial protein expression system as described previously.[23] Gallium-metalated sulfonated corrole was synthesized, reconstituted in phosphate-buffered saline (PBS), and quantified as described previously.[12] HerGa, HerGa-2 and HerGa-3 complexes were assembled by combining each protein and S2Ga at corrole:protein ratios of 30, 5, or 8, respectively, and incubating mixtures with gentle agitation on ice for 1 h, followed by ultrafiltration through a 50 kDa MWCO filter column (Millipore, Billerica, MA, USA) that had been coated with 10% glycerol. The column was spun at 1000*g* until the filtrate clarified and the volume was reduced to <500 μL. Concentrations used for cell treatments are based on the corrole concentration in each complex, determined by obtaining the λ_{max} absorption using UV/vis spectroscopy and applying the following equation: (absorbance at λ_{max}/corrole extinction coefficient) × dilution factor = concentration (M).

Cells. MDA-MB-435 cells were obtained from the National Cancer Institute and maintained at 37 °C in DMEM, 10% fetal bovine serum at 5% CO_2. All cell treatments were performed at ~36 h after plating to allow sufficient receptor re-expression and display on the cell surface.

Live Cell Microscopy of Internalized Reagents. At ~36 h after MDA-MB-435 cells were plated in delta T chambers (10^5/well), the medium was replaced with HBSS containing 1 μM HerGa or S2Ga, followed immediately by acquisition of confocal images every 5 min. To image HerGa internalization ∓ paclitaxel, confocal images were acquired at different depths (~10 μm sections at 1 μm steps) every 5 min for 1 h. Excitation and emission wavelengths at 560 nm and 620 nm ± 20 nm, respectively, were selected for HerGa detection.

Cell Death Dose Curve. Cells were plated at 10^4 cells per well in a 96 well dish. 36 h later the medium was aspirated and replaced with 50 μL of complete DMEM containing the indicated concentrations of HerGa. The cells were rocked at 37 °C for four hours, after which an additional 50 μL of complete medium was added and cells continued incubation at 37 °C without rocking. Twenty-four hours after the start of the treatment the cell number was determined by the crystal violet (CV) assay. Briefly, the medium was aspirated and cells were washed with PBS containing 0.01% Mg^{2+} and 0.01% Ca^{2+}. The PBS was aspirated, and each well was stained with 0.1% Crystal Violet at RT for 15 min. The cells were then washed in PBS with Mg^{2+}/Ca^{2+} 4 times. After the final wash, each well received 100 μL of 95% ethanol to release the CV. The plate was incubated at RT for 10 min before the absorbance at 590 nm was measured.

Mitochondrial Membrane Potential Measurement. The distribution of the cationic dye, tetramethyl rhodamine methyl ester (TMRM), across the mitochondrial membrane is governed primarily by the Nernst equation,[24] whereas transmembrane potential collapse results in its diffusion into the cytosol, thus reducing its intracellular fluorescence intensity.[25] MDA-MB-435 cells were plated in Delta T chambers at 10^4 cells/chamber and incubated for 36 h, after which medium was aspirated from each chamber and replaced with 0.5 mL of fresh complete medium containing HerGa, S2Ga, HerPBK10, or PBS at the indicated concentrations. Each chamber was rocked for 4 h at 37 °C, 5%

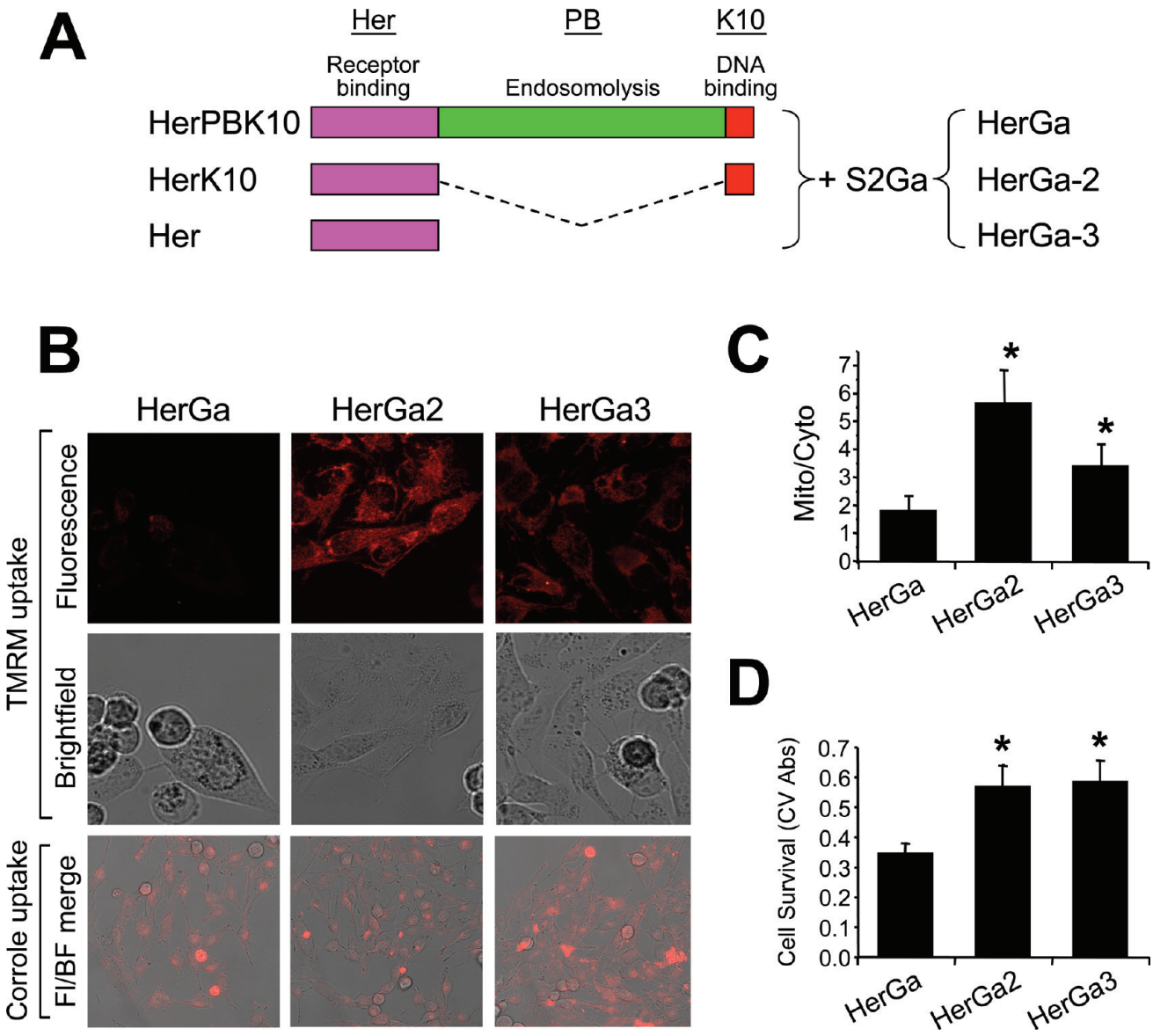

Figure 3. $\Delta\Psi$(m) disruption requires endosome escape. (A) Linear protein domain map comparing HerPBK10 and endosomolytic-deficient derivatives. Each protein is shown from carboxy (left) to amino (right) terminus, respectively. Complexes made from combining S2Ga with truncated proteins, HerK10 and Her, are designated HerGa-2 and HerGa-3, and are compared to parental HerGa for the effect of each on mitochondrial uptake of TMRM and cell survival. (B) TMRM and complex uptake in MDA-MB-435 cells. Cells were treated with 1 μM (final corrole dose) of each complex for 24 h before medium exchange and imaging. Where indicated, the medium was replaced with 20 nM TMRM in PBS and imaged after mitochondrial TMRM accumulation reached equilibrium (~1 h). Both TMRM and corrole uptake images were collected by two-photon excited confocal fluorescence microscopy. Fluorescence micrographs show *z*-stacked maximum intensity projections of acquired images. Fl/BF, Fluorescence-brightfield overlay. (C) Quantification of TMRM uptake in panel B (see Materials and Methods). (D) Relative cell survival (determined by crystal violet stain; see Materials and Methods) after treatment in panel B. *, $P < 0.05$ compared to HerGa (two-tailed unpaired *t* test).

CO_2 and then received 0.5 mL of additional medium, bringing the final volume to 1 mL, after which chambers were incubated another 20 h. The medium was then aspirated and replaced with 20 nM TMRM in PBS, and two-photon excited confocal TMRM fluorescence images were acquired at different *z*-depths after TMRM accumulation reached equilibrium (~1 h). Mitochondrial membrane potential was quantified from a *z*-stacked maximum intensity projection of each acquired image by calculating the fluorescence intensity ratio of mitochondrial to cytoplasm sites.[10,11] In calculating the mitochondria/cytoplasm ratio, average fluorescence intensity for 10 different mitochondrial regions and one mitochondria-free region (distinguishing the cytoplasm) within the same cells were measured respectively. This calculation was performed for all cells in each field of view from three independent experiments.

Fluorescence Lifetime Detection. Fluorescence lifetime imaging was performed using a femtosecond (fs) pulsed laser (Mai Tai, Spectra Physics) light tuned to 424 nm, at a repetition rate of 80 MHz, generated by the second harmonic of a fs pulsed laser at 848 nm in a Beta Barium Borate (BBO) crystal, delivered to a Nikon microscope through macro lenses, a diffuser, a band-pass filter (425 ± 5 nm), and several mirrors. The delivered light was reflected to the back focal plane of a 100× objective (Nikon 100× planfluor, NA: 1.3) for the excitation of the HerGa.

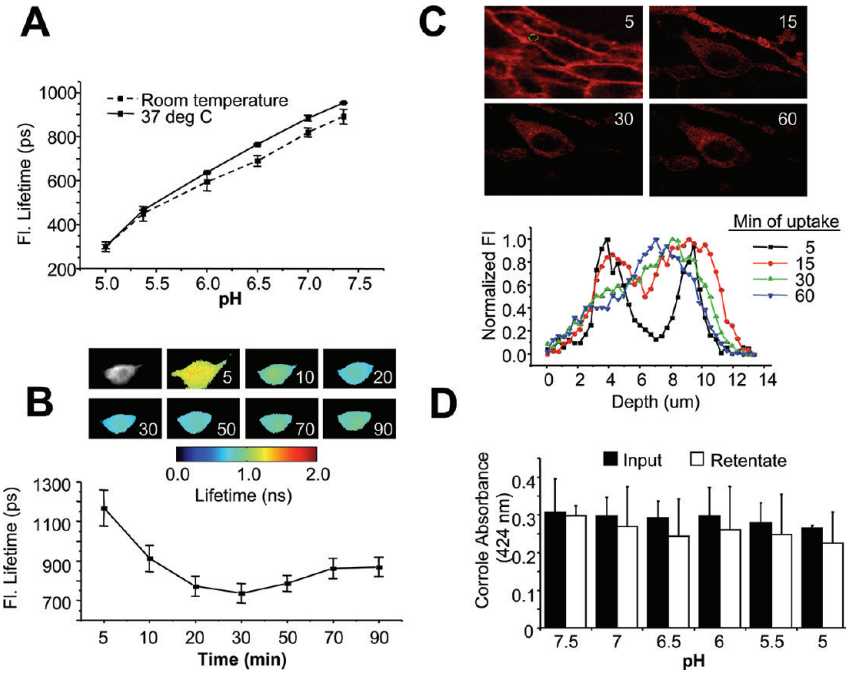

Figure 4. Effect of pH on corrole retention and fluorescence lifetime. (A) Measurement of HerGa fluorescence lifetime in titrating pH buffers. Fluorescence lifetime of 25 μM HerGa solutions in different pH (5.0, 5.5, 6.0, 6.5, 7.0, and 7.5) was measured at room temperature and 37 °C respectively, in a cell-free system. During the measurements, the temperature was strictly (~0.1 °C) controlled by a ΔT culture dish system. Before adding the corroles to the chamber, the pH of each corrole solution was confirmed with a pH meter. (B) Monitoring fluorescence lifetime changes of HerGa during uptake into MDA-MB-435 cells. Fluorescence lifetime images of HerGa were acquired at different time points (5, 10, 20, 30, 50, 70, and 90 min) after addition of 25 μM HerGa into the delta T chamber containing attached MDA-MB-435 cells. A total of 25 images were acquired (0−4800 ps; time step, 200 ps; gate width, 600 ps; ex, 424 nm; light pulse width, 100 fs). The images were analyzed (lower graph) using the first order exponential decay fitting method. (C) Monitoring HerGa fluorescence as a reflection of uptake kinetics. Two-photon fluorescence imaging-enabled acquisition and analysis of HerGa (25 μM) at various depths during uptake in MDA-MB-435 cells. Images were acquired at different time points of HerGa uptake (5, 15, 30, and 60 min after addition to cells) and at different z-depths with a step size of 350 nm (ex, 780 nm; em, 600−650 nm). Micrographs show images at 6 μm depth at indicated time points during HerGa uptake. The graph shows the fluorescence intensity z-depth profile of the region selected by a dotted circle in the first micrograph. (D) Evaluating corrole retention under decreasing pH conditions. The acidity of a HEPES-buffered saline solution was adjusted to the indicated pH levels, and preassembled HerGa was added to each pH buffer and incubated for 30 min at room temp (in a cell-free system), followed by filtration through 10K MWCO membranes to remove any released corrole. The absorbances at 424 nm (maximum absorbance wavelength of gallium corrole) were obtained from the preassembled complex before incubation with each pH buffer ("Input"), and the filtered complex was recovered from the ultrafiltration device after incubation with each pH buffer ("Retentate"). Error bars represent SD of repeat experiments. N = 2−3 samples/pH per experiment.

Fluorescence emission from HerGa was collected by the objective and delivered onto a CCD connected with time-gated intensifier (TGI) (Lavison) through an emission filter (620 ± 60 nm), and then fluorescence lifetime images of HerGa were acquired at indicated points.

Superoxide Detection. MDA-MB-435 grown in 96-well plates at 1 × 10^4/well for 36 h were aspirated of medium and received fresh medium containing HerGa or S2Ga (at 1 μM corrole concentration), HerPBK10 (at equivalent protein concentration to HerGa), or PBS (mock), followed by incubation for 1 h at 37 °C. The cells were then assayed for superoxide generation by measuring luminol oxidation following a commercial procedure (LumiMax Superoxide Anion detection kit; Agilent Technologies, Santa Clara, CA, USA). Light emission was recorded every 1 min for 30 min by a Veritas Microplate Luminometer (Promega Corporation, Sunnyvale, CA, USA). Where indicated, cells were preincubated in Tiron at the indicated concentrations for 1 h before treatment. Superoxide detection in a cell-free system was performed by adding 1 μM HerGa or S2Ga, HerPBK10 (at equivalent protein concentration to HerGa), or PBS directly to assay medium at 100 μL final volume in separate wells of a 96-well plate, and wells were processed as described earlier to measure superoxide.

Immunofluorescence. Cells were treated with HerGa or individual components as indicated and then processed for immunofluorescent histochemical staining following our previously established procedures.[26] Where indicated, fixed cells were incubated for 1 h with antibodies against actin (to assess microfilaments) or tubulin (to assess microtubules). Samples were imaged by laser scanning fluorescence confocal microscopy as described earlier.[3]

Paclitaxel Treatment. MDA-MB-435 cells plated in Delta T chambers (10^4/chamber) received the following treatments at 36 h after plating: medium was replaced with 0.5 mL of medium containing HerGa (1 μM), the equivalent volume of PBS (Mock), or HerGa + 5 μM paclitaxel (after a 15 min paclitaxel pretreatment, as previously described).[26] All treatments included 0.25% DMSO. The chambers were rocked for 4 h at 37 °C, 5% CO_2, followed by supplementation with an additional 0.5 mL of medium and a further 20 h incubation. Separate experimental treatments were independently assessed for TMRM uptake and superoxide levels as described earlier.

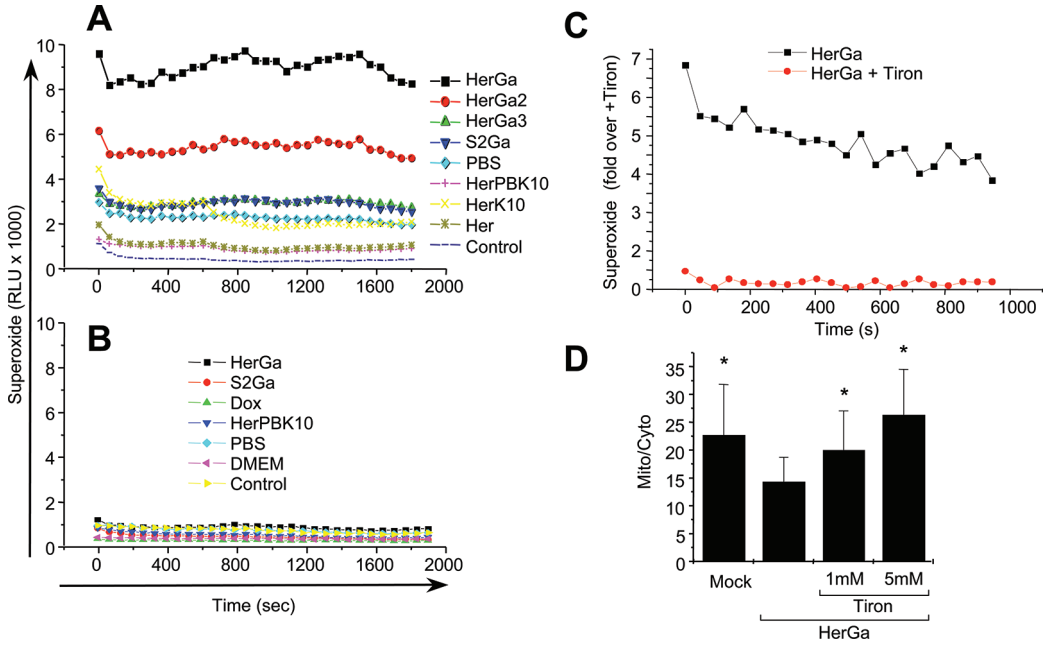

Figure 5. Cytosolic HerGa induces superoxide generation. MDA-MB-435 cells treated with 1 μM HerGa, S2Ga, HerPBK10, or PBS (mock) for 1 h were analyzed for superoxide via chemiluminescence detection (see Materials and Methods). Graphs (A−C) display relative luminescence unit (RLU) decay over time. (A) Contribution of endosomolysis on superoxide generation. MDA-MB-435 cells were treated and assayed for chemiluminescence as described earlier. HerGa, HerGa-2, HerGa-3, and S2Ga were added to cells at 1 μM corrole concentration. Individual components were added at the equivalent protein concentration to each respective complex. (B) Lack of superoxide generation in a cell-free system. HerGa (1 μM) and equivalent concentrations of S2Ga, HerPBK10, or PBS were added directly to superoxide anion assay medium and luminol oxidation was measured as described in the Materials and Methods. (C) Reduction of HerGa-mediated superoxide generation in MDA-MB-435 cells by the superoxide scavenger, Tiron. Cells were incubated with 1 mM Tiron for 1 h before treatment with 1 μM HerGa for 24 h, followed by superoxide measurement as described earlier. (D) Effect of Tiron on HerGa-mediated $\Delta\Psi$(m) disruption. Cells were incubated with the indicated concentrations of Tiron before treatment with 1 μM HerGa for 24 h, followed by measurement of TMRM uptake as described earlier. *, $P < 0.02$ compared to HerGa alone, as determined by two-tailed unpaired t test.

RESULTS

HerPBK10 Is Required for Corrole Internalization and Cytotoxicity. Evaluation of cellular uptake was performed by confocal fluorescence microscopy of live HER2+ MDA-MB-435 cells and examination of intracellular corrole fluorescence over time. The results show that HerGa (1 μM) undergoes internalization within minutes, whereas free untargeted corrole (S2Ga) at equivalent concentration (1 μM) displays no detectable accumulation microscopically (Figure 1A) and by measurement of intracellular fluorescence intensity (Figure 1C). Even at 1 h after initial administration to cells, intracellular S2Ga fluorescence was not detectable, whereas it was very pronounced for HerGa treated cells (Figure 1B). A direct relationship between these findings and cytotoxicity was elucidated from *in vitro* dosed toxicity analyses performed 24 h after incubation, showing that cell death plateaus at concentrations at and above 10 nM HerGa, with a CD50 of ~0.5 nM (Figure 1D). This contrasts with the same analysis of S2Ga, which is not toxic up to 100 μM over the same time frame (Figure 1D).

Cytosolic HerGa Compromises Mitochondrial Membrane Potential . Based on the previous findings, we examined whether HerGa directly impacts mitochondria by using a Nernstian dye, tetramethyl rhodamine methyl ester (TMRM), to investigate the $\Delta\Psi$(m) of HerGa-treated MDA-MB-435 cells. In contrast to mock treatment, HerGa significantly reduced the ratio of mitochondrial to cytosolic intensity by 24 h after treatment, while HerPBK10 or S2Ga alone had little effect (Figure 2A,B). The onset of $\Delta\Psi$(m) collapse could be detected as soon as 1 h after HerGa treatment (Figure 2B), suggesting a fairly early mitochondrial impact after uptake.

To determine whether endosomal escape is required to facilitate $\Delta\Psi$(m) disruption, we compared HerGa to similar complexes (designated HerGa-2 and HerGa-3) made with carrier protein (HerK10 and Her, respectively) lacking the endosomal-disrupting penton base domain (Figure 3A).[23] In contrast to the reduced TMRM uptake in HerGa-treated cells, HerGa-2 and HerGa-3 at equivalent corrole dose (1 μM) had negligible effect (Figure 3B,C; $P < 0.05$ compared to HerGa), despite the ability of HerGa-2 and HerGa-3 to internalize into target cells (Figure 3B, lower panels). HerGa-2 and HerGa-3 also were not cytotoxic to treated cells, in contrast to the significant reduction in cell survival induced by parental HerGa (Figure 3D; $P < 0.05$ compared to HerGa), altogether indicating that $\Delta\Psi$(m) disruption requires direct exposure to HerGa, and leads to cell death.

HerGa Avoids a Highly Acidic Microenvironment after Cell Entry. Our recent studies indicate that corrole fluorescence lifetime is altered during cell uptake,[27] and specifically shortens in direct relation to microenvironmental pH when tested under controlled pH conditions (Figure 4A). We took advantage of this property to determine the timing of endosome escape. During cellular uptake of HerGa, the corrole fluorescence lifetime exhibited a time-dependent decrease (Figure 4B) that correlated with a transition from a neutral to mildly acidic (pH ~6.5) microenvironment within the first 15 min of uptake (Figure 4A), but did not decrease below ~700 ps, thus avoiding a highly acidic

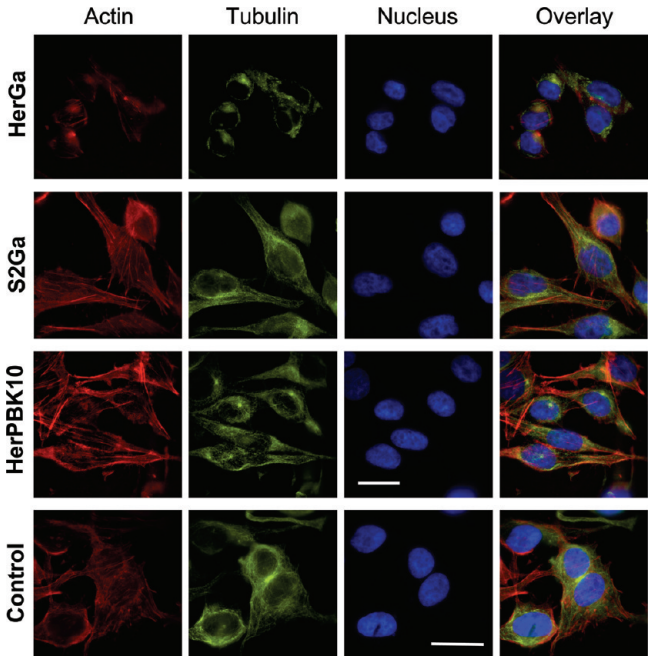

Figure 6. HerGa disrupts the cytoskeleton. MDA-MB-435 cells treated with S2Ga or HerGa at 1 μM final corrole concentration, or HerPBK10 alone at equivalent protein concentration to HerGa, were assessed for cytoskeletal changes by 24 h of treatment by fluorescence labeling of actin (red) or tubulin (green). Blue, nucleus. Epifluorescence imaging was performed using filter cubes to detect DAPI (ex, 380 nm; em, 400 nm), FITC (ex, 488 nm; em, 530 nm), CY3 (ex, 550 nm; em, 580 nm), and corrole (ex, 425 nm; em, 620 nm), and images collected by a 40× objective (Nikon Planfluor, NA: 0.75). To increase image contrast, background subtraction from each acquired image was performed using ImageJ. Bar, ~20 μm.

(pH <6.5) compartment (Figure 4B). To confirm whether this is indicative of early endosomal escape, we used two-photon fluorescence live cell imaging to monitor fluorescence yield and transit of HerGa during uptake. Intracellular depth analysis shows that HerGa is localized closer to the cell periphery (shown as two fluorescence peaks at 4 and 10 um depths) early (5 min) after uptake correlating with an increase in fluorescence intensity, indicative of sequestration into membrane-juxtaposed vesicles (Figure 4C). Later time points show HerGa transiting deeper within the cell, away from the plasma membrane (indicated by a single peak at ~7 μm by 1 h) (Figure 4C), concomitant with a reduction in fluorescence yield that is indicative of diffusion from vesicles. Taken together with the earlier findings using the endosomolytic-deficient mutants, these results provide comprehensive evidence that HerGa escapes relatively early from endosomal vesicles, thus avoiding entry into highly acidic compartments.

Low pH Does Not Induce Corrole Release from the Carrier. We performed a *cell-free* assay to determine whether S2Ga separates from HerPBK10 in different pH buffers adjusted to mimic a neutral/extracellular environment (7.5−7.0), mildly acidic environment such as that in the early endosome or tumor microenvironment (6.5−6.0), and moderately acidic environment such as that in late endosomes/lysosomes (5.5−5.0). Our results show that a pH decrease, even to values as low as 5.0, did not yield detectable corrole release from the carrier protein (Figure 4D). Taken together with the previous endosomolytic and pH analyses, these findings suggest that the acidic endosomal microenvironment is insufficient to induce corrole release from the HerPBK10 carrier protein during uptake.

Cytosolic HerGa Elevates Intracellular Superoxide. We assessed the contribution of reactive oxygen species (ROS) in the cell death mechanism of HerGa by using a luminol substrate to detect superoxide (O_2^-) in MDA-MB-435 cells after exposure to HerGa (1 μM) or individual components (HerPBK10 and S2Ga alone) for 1 h. While HerPBK10 and S2Ga alone had a minor to negligible effect on luminescence over mock (PBS) treatment, and all three compounds induced low levels of luminescence over untreated (control) cells, HerGa induced the highest levels (3−5× the elevation of mock treatment) (Figure 5A), suggesting that considerable O_2^- is generated by HerGa treatment. To assess whether O_2^- generation is due to any innate catalytic activity, we repeated this assay in cell-free conditions. Our results showed that none of the reagents used here produced detectable luminescence under these conditions (Figure 5B), indicating that O_2^- generation occurs as a cellular response to HerGa treatment. To evaluate the contribution of endosomolysis on O_2^- generation, we measured luminescence from cells after treatment with the endosomolytic-defective complexes, HerGa-2 and HerGa-3. Both HerGa-2 and HerGa-3 exhibited considerably lower luminescence compared to HerGa, with HerGa-3 yielding no detectable luminescence over mock treatment, indicating that endosomal escape is necessary for HerGa-mediated O_2^- generation. To assess the contribution of O_2^- generation to mitochondrial damage, we evaluated HerGa-mediated $\Delta\Psi(m)$ changes in the presence of the superoxide scavenger, Tiron, which sufficiently reduces and prevents O_2^- generation at 1−5 mM (Figure 5C), in agreement with established studies.[28] Here, Tiron restored normal $\Delta\Psi(m)$ in HerGa-treated cells in comparison to HerGa-treatment without Tiron (Figure 5D), indicating that HerGa-induced O_2^- contributes to $\Delta\Psi(m)$ disruption.

HerGa-Mediated Cytoskeletal Disruption Occurs Downstream of Superoxide Elevation. We examined the cytoskeletal effect of HerGa uptake by immunofluorescence analysis of treated MDA-MB-435 cells and observed that, in comparison to the normal broad cytosolic distribution of actin filaments and microtubules as seen in mock and control (S2Ga and HerPBK10 alone) treated cells, HerGa (1 μM) induced considerable cytoskeletal collapse by 24 h after uptake (Figure 6). To distinguish whether cytoskeletal disruption resulted as a direct impact from HerGa or as a downstream event of cell damage, we used the microtubule stabilizer, paclitaxel, to assess whether preventing microtubule breakdown would affect $\Delta\Psi(m)$ disruption and O_2^- elevation. Paclitaxel significantly reduced HerGa-induced $\Delta\Psi(m)$ breakdown ($P < 0.0001$ compared to HerGa) (Figure 7A) and O_2^- generation (Figure 7B), suggesting that cytoskeletal disruption leads to ROS and mitochondrial damage. However, the oxygen scavenger, Tiron, prevented HerGa-mediated cytoskeletal breakdown (Figure 8), thus suggesting that HerGa causes ROS-mediated cytoskeletal damage. To reconcile which events are causative, we examined the stage of HerGa uptake (detected by intracellular corrole fluorescence) affected by paclitaxel treatment. Our findings show that paclitaxel reduces intracellular accumulation by nearly 70%, (Figure 7C,D), indicating that microtubule stabilization prevents uptake/intracellular transit of HerGa, which in turn prevents the downstream events of ROS generation, and ROS-mediated damage to mitochondria and the cytoskeleton. These findings also indicate that dynamic microtubules are required for mediating HerGa uptake.

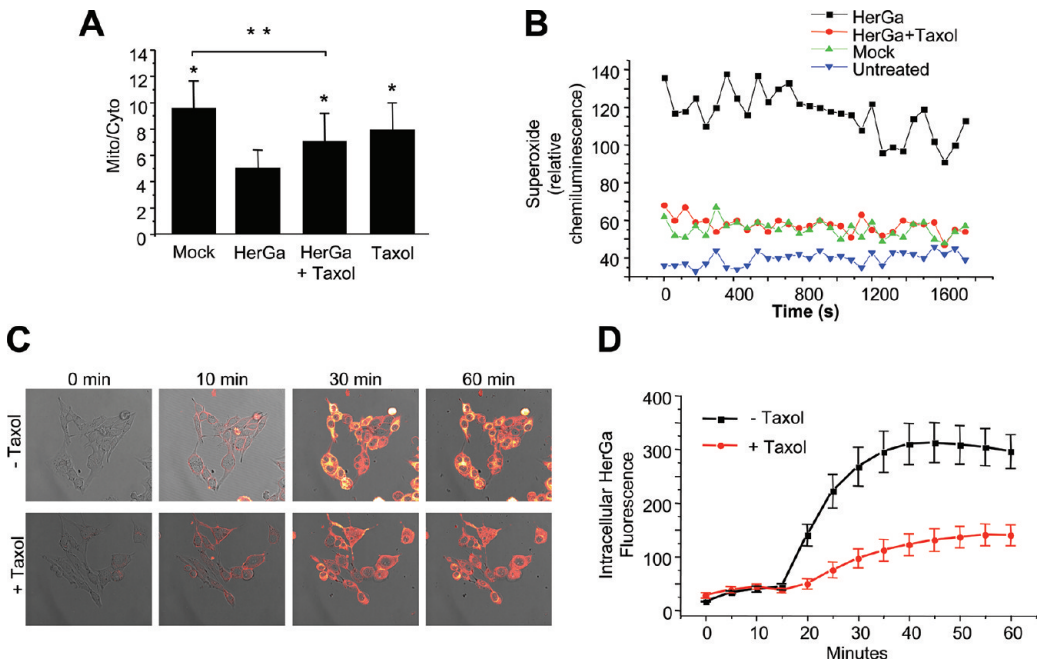

Figure 7. Microtubule stabilization abrogates events downstream of HerGa uptake. MDA-MB-435 cells were incubated in medium containing 5 μM paclitaxel for 15 min before exposure to HerGa (see Materials and Methods). At 24 h after exposure, cells received (A) 20nM TMRM and were monitored for mitochondrial TMRM accumulation as described previously; or (B) luminol and assayed for superoxide levels as described in the Materials and Methods. *, $P < 0.0001$ compared to HerGa treatment. **, $P < 0.0001$. Statistical significances determined by two-tailed unpaired t tests. (C, D) Effect of paclitaxel on HerGa uptake. (C) Confocal images were acquired of live MDA-MB-435 cells after treatment with 5 μM HerGa (∓ pretreatment with 5 μM paclitaxel; see Materials and Methods). (D) Cytosolic fluorescence from the same cell region per time point was measured, and average fluorescence variations were plotted over time, comparing HerGa ∓ paclitaxel.

DISCUSSION

Our previous studies have established that HerGa binds target HER2+ cells *in vitro* specifically through HER ligation, as confirmed through competitive inhibition by free ligand, and undergoes receptor-mediated endocytosis in response to receptor binding.[12] These same studies also showed that HerPBK10 enabled corrole toxicity at low (submicromolar) doses in contrast to the free corrole (not attached to HerPBK10), which required daily doses as high as 35 μM for 3 days to induce appreciable cytotoxicity. These previous studies suggest that the relatively low dose required for HerGa therapeutic efficacy is due to the known internalization and membrane-penetration attributes of HerPBK10 that also enable gene delivery elsewhere,[23] while the inability of the free corrole to penetrate the cell membrane prevents effective toxic impact on target cells, even if it can undergo endocytosis through attachment to or co-uptake with serum proteins.[12] In support of that hypothesis, we show here that HerGa undergoes internalization, as seen by the accumulation of intracellular corrole fluorescence over time, whereas free, untargeted corrole (S2Ga) at equivalent concentration (1 μM) showed no detectable accumulation microscopically. Correspondingly, HerGa elicited cytotoxicity whereas S2Ga did not, altogether indicating that HerPBK10 is needed for corrole internalization and mediating corrole toxicity, especially at low and pharmacologically relevant doses.

One unexpected discovery while conducting these studies has been the direct relationship between HerGa fluorescence lifetime and pH. This unique property has been useful here for reporting the intracellular environmental conditions during uptake and could possibly be exploited in future studies for diagnostic monitoring of the microenvironment *in vivo*. Together with two-photon imaging and intracellular depth analysis, the fluorescence lifetime

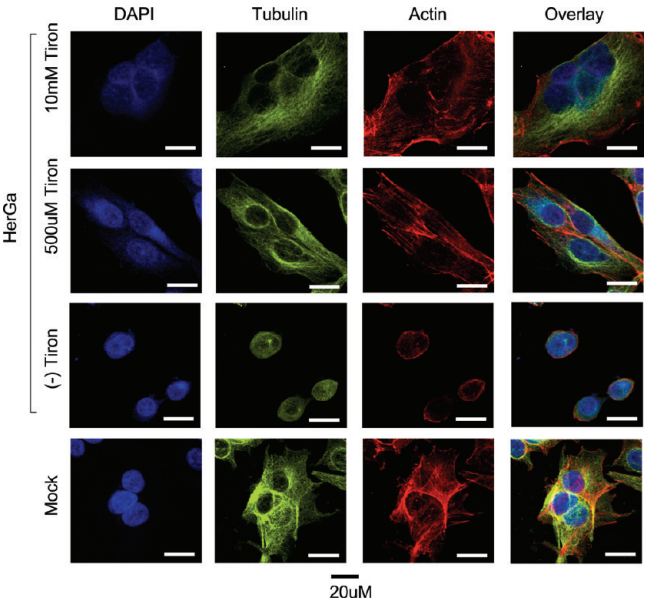

Figure 8. HerGa-mediated superoxide generation disrupts the cytoskeleton. Where indicated, MDA-MB-435 cells were incubated with the indicated concentrations of Tiron for 1 h before treatment with 1 μM HerGa or Mock (PBS) treatment for 24 h, followed by fixation and immunofluorescence processing to label actin (red), tubulin (green), and nuclei (blue). Cells were imaged as described in Figure 6. Bar, ~20 μm.

changes of HerGa during cell uptake indicate that HerG accumulates into membrane-juxtaposed vesicles of slightly acidic pH, followed by transit away from the plasma membrane and deeper within the cell that corresponds to escape from endosomal vesicles. Cytosolic exposure would enable HerGa to transit along cytoskeletal pathways connecting the plasma ?A3B2 tlsb?>membrane to organelles, including the mitochondria. In agreement, the paclitaxel-mediated reduction of intracellular HerGa indicates that dynamic microtubules are required for initial transit into the cell and throughout the cytoplasm. The prevention of $\Delta\Psi(m)$ disruption and O_2^- elevation by paclitaxel also indicates that the cytoskeletal network is necessary for transport of HerGa to the proximity of oxygen sources, such as the mitochondria. The prevention of cytoskeletal collapse by Tiron indicates that HerGa-mediated actin and tubulin disruption lies downstream of O_2^- elevation. These findings altogether suggest that the cytoskeletal network is necessary to provide the initial means of HerGa transport in the cell to oxygen-generating sources (such as the mitochondria) where HerGa-mediated O_2^- elevation takes place, and as a result, ultimately becomes a target of oxidative damage.

Another unexpected finding was that a pH as low as 5.0 does not induce corrole release from the HerGa complex, thus suggesting that the environment encountered through receptor-mediated endocytosis and endocytic maturation does not affect complex integrity. Either the corrole stays bound to the carrier throughout cell entry or it is released through a pH-independent process. Whereas a microscopic analysis of corrole release from HerGa in cells could verify these findings, the processing required for immunofluorescence assay has produced fixation artifacts showing false nuclear accumulation of corrole fluorescence (not shown), thus confounding appropriate evaluation.

Here we find that HerGa, but not its individual constituents, induces $\Delta\Psi(m)$ collapse that is mediated through the elevation of superoxide. Moreover, we find through the use of endosomolytic-deficient mutants that direct exposure of HerGa to the cytosol is necessary for these events to occur. Taken altogether, these studies have identified the following stepwise pathway mediating the cytotoxic mechanism of HerGa: HerPBK10 is required to mediate uptake (Figure S1 in the Supporting Information, step a) and early endosomal release (Figure S1 in the Supporting Information, step b), thus enabling HerGa to avoid low pH compartments such as the late endosome and lysosome after cell entry. Cytosolic entry is necessary to facilitate downstream O_2^- elevation (Figure S1 in the Supporting Information, step c), which in turn mediates both cytoskeletal and $\Delta\Psi(m)$ disruption (Figure S1 in the Supporting Information, steps d and e). As superoxide generation would cause oxidative damage to cellular processes and structures, and $\Delta\Psi(m)$ loss would disrupt cellular metabolic activity, these specific phenomena explain how HerGa mediates death to target cells.

How HerGa directly interacts with the mitochondrion to elicit these cell death mediators remains to be elucidated. Consistent with observations in our previous studies,[3,12] corrole fluorescence is observable throughout the cytoplasm after HerGa uptake and is not necessarily specifically targeted to mitochondria. Given the structural similarity of corroles to porphyrins, HerGa may indirectly affect mitochondrial ROS levels by activating the mitochondrial benzodiazapine receptor, for which several porphyrins are endogenous ligands.[29] On the other hand, HerGa could impact extramitochondrial sources of superoxide generation, including NADPH oxidase on the plasma membrane and cytoplasmic enzymes such as xanthine oxidase and nitric oxide synthase,[30] which could lead to mitochondrial damage as well as other downstream apoptotic-like events. Our cell-free studies show that the corrole itself cannot directly catalyze ROS generation, hence interactions with host factors are required.

Whereas ROS can activate the intrinsic apoptotic pathway,[31] our initial investigations on the contribution of apoptosis have yielded atypical findings. Mitochondrial permeabilization typically releases cytochrome *c*, which activates the caspase cascade resulting in cell death. Here, moderate but significant elevation in DNA fragmentation, an indicator of apoptotic cell death, was observed in HerGa but not control-treated cells (Figure S2A in the Supporting Information). However, other "classical" markers of apoptosis were lacking, including phosphatidylserine (PS) externalization (Figure S2A in the Supporting Information), and elevation of activated caspase 9 and 3 (Figure S2B in the Supporting Information). Moreover, cytochrome *c* release was not detected unless the cells were exposed to HerGa at a 10-fold higher dose over the therapeutic range (Figure S2C in the Supporting Information). Alternative cell death pathways may account for these anomalies. For example, caspase-independent fragmentation of DNA in the absence of PS exposure has been observed in HER2+ T-47D tumor cells undergoing autophagy.[32] Elsewhere, selective release of Smac/DIABLO and Omi/HtrA2, but not cytochrome *c*, from mitochondria can result from S100A8/A9-induced death in tumor cells.[33] Mitochondrial release of Smac/DIABLO has been observed in cells undergoing anchorage-dependent cell death, or anoikis,[34] and can function independently of cytochrome *c*.[35] Importantly, Schafer et al.[36] demonstrated that antioxidants inhibit anoikis in breast cancer cells, suggesting that elevated ROS are required in detachment-mediated cell death. These examples indicate that further studies are warranted for determining the contribution of nonclassical cell death pathways to HerGa-mediated toxicity, and they are currently ongoing.

Given our recent successful demonstration that targeted corroles eliminate tumor growth,[3] the investigations presented here shed light on the mechanism of corrole-mediated cell death. These studies will direct our future efforts in engineering modifications into the corrole and carrier protein that may enable even greater potency and specificity for tumor cells, thus yielding a therapeutic with optimized efficacy and safety.

■ ASSOCIATED CONTENT

Supporting Information. A graphical summary of the mechanism elucidated from this study and evaluation of apoptotic markers. This material is available free of charge via the Internet at http://pubs.acs.org.

■ AUTHOR INFORMATION

Corresponding Author

*Department of Biomedical Sciences, Cedars-Sinai Medical Center, 8700 Beverly Blvd., Los Angeles, CA 90048. E-mail: medinal@cshs.org. Tel: 310-423-7339.

■ ACKNOWLEDGMENT

L.K.M.-K. thanks J.C., D.R., and M.M.-K. for continued support. This work was supported by grants to L.K.M.-K. from the NIH (R21 CA116014, R01 CA102126, R01 CA129822, and R01 CA140995), the DoD (BC050662), the Susan G. Komen

Breast Cancer foundation (BCTR0201194), and the Donna and Jesse Garber Award. Work at Caltech was supported by NIH DK019038 and the Arnold and Mabel Beckman Foundation. Work at the Technion was supported by The Herbert Irving Cancer and Atherosclerosis Research Fund.

REFERENCES

(1) Dougherty, T. J.; Gomer, C. J.; Henderson, B. W.; Jori, G.; Kessel, D.; Korbelik, M.; Moan, J.; Peng, Q. Photodynamic therapy. *J. Natl. Cancer Inst.* **1998**, *90*, 889–905.

(2) Via, L. D.; Magno, S. M. Photochemotherapy in the treatment of cancer. *Curr. Med. Chem.* **2001**, *8*, 1405–1418.

(3) Agadjanian, H.; Ma, J.; Rentsendorj, A.; Valluripalli, V.; Hwang, J. Y.; Mahammed, A.; Farkas, D. L.; Gray, H. B.; Gross, Z.; Medina-Kauwe, L. K. Tumor detection and elimination by a targeted gallium corrole. *Proc. Natl. Acad. Sci. U.S.A.* **2009**, *106* (15), 6105–10.

(4) Agadjanian, H.; Ma, J.; Rentsendorj, A.; Sorasaenee, K.; Hwang, J. Y.; Weaver, J.; Valluripalli, V.; Moats, R.; Farkas, D.; Gray, H.; Gross, Z., Medina-Kauwe; L. K. Corrole conjugates: a unique approach to tumor targeting Presented at *The American Association for Cancer Research 2008 Annual Meeting*, 2008, 2328.

(5) Kanamori, A.; Catrinescu, M. M.; Mahammed, A.; Gross, Z.; Levin, L. A. Neuroprotection against superoxide anion radical by metallocorroles in cellular and murine models of optic neuropathy. *J. Neurochem.* **2010**, *114* (2), 488–98.

(6) Kupershmidt, L.; Okun, Z.; Amit, T.; Mandel, S.; Saltsman, I.; Mahammed, A.; Bar-Am, O.; Gross, Z.; Youdim, M. B. Metallocorroles as cytoprotective agents against oxidative and nitrative stress in cellular models of neurodegeneration. *J. Neurochem.* **2010**, *113* (2), 363–73.

(7) Haber, A.; Aviram, M.; Gross, Z. Protecting the beneficial functionality of lipoproteins by 1-Fe, a corrole-based catalytic antioxidant. *Chem. Sci.* **2011**, *2*, 295–302.

(8) Okun, Z.; Kupershmidt, L.; Amit, T.; Mandel, S.; Bar-Am, O.; Youdim, M. B.; Gross, Z. Manganese corroles prevent intracellular nitration and subsequent death of insulin-producing cells. *ACS Chem. Biol.* **2009**, *4* (11), 910–4.

(9) Haber, A.; Mahammed, A.; Fuhrman, B.; Volkova, N.; Coleman, R.; Hayek, T.; Aviram, M.; Gross, Z. Amphiphilic/Bipolar Metallocorroles that Catalyze the Decomposition of Reactive Oxygen and Nitrogen Species, Rescue Lipoproteins from Oxidative Damage, and Attenuate Atherosclerosis in Mice. *Angew. Chem., Int. Ed.* **2008**, *16*, 16.

(10) Paolesse, R. Syntheses of Corroles. In *The Porphyrin Handbook*; Kadish, K. M., Smith, K. M., Guilard, R., Eds.; Academic Press: New York, 2000; Vol. II, pp 201−232.

(11) Sessler, J. L.; Weghorn, S. J. *Expanded, Contracted, & Isomeric Porphyrins*; Pergamon: Oxford, 1997; p 1−9.

(12) Agadjanian, H.; Weaver, J. J.; Mahammed, A.; Rentsendorj, A.; Bass, S.; Kim, J.; Dmochowski, I. J.; Margalit, R.; Gray, H. B.; Gross, Z.; Medina-Kauwe, L. K. Specific delivery of corroles to cells via noncovalent conjugates with viral proteins. *Pharm. Res.* **2006**, *23* (2), 367–77.

(13) Bacus, S. S.; Zelnick, C. R.; Plowman, G.; Yarden, Y. Expression of the erbB-2 family of growth factor receptors and their ligands in breast cancers. Implication for tumor biology and clinical behavior. *Am. J. Clin. Pathol.* **1994**, *102* (4 Suppl. 1), S13–24.

(14) Holmes, W. E.; Sliwkowski, M. X.; Akita, R. W.; Henzel, W. J.; Lee, J.; Park, J. W.; Yansura, D.; Abadi, N.; Raab, H.; Lewis, G. D.; et al. Identification of heregulin, a specific activator of p185erbB2. *Science* **1992**, *256* (5060), 1205–10.

(15) Slamon, D. J.; Clark, G. M.; Wong, S. G.; Levin, W. J.; Ullrich, A.; McGuire, W. L. Human breast cancer: correlation of relapse and survival with amplification of the HER-2/neu oncogene. *Science* **1987**, *235* (4785), 177–82.

(16) Slamon, D. J.; Clark, G. M. Amplification of c-erbB-2 and aggressive human breast tumors? *Science* **1988**, *240* (4860), 1795–8

(17) van der Horst, E. H.; Weber, I.; Ullrich, A. Tyrosine phosphorylation of PYK2 mediates heregulin-induced glioma invasion: novel heregulin/HER3-stimulated signaling pathway in glioma. *Int. J. Cancer* **2005**, *113* (5), 689–98.

(18) Lewis, G. D.; Lofgren, J. A.; McMurtrey, A. E.; Nuijens, A.; Fendly, B. M.; Bauer, K. D.; Sliwkowski, M. X. Growth regulation of human breast and ovarian tumor cells by heregulin: Evidence for the requirement of ErbB2 as a critical component in mediating heregulin responsiveness. *Cancer Res.* **1996**, *56* (6), 1457–65.

(19) Gregory, C. W.; Whang, Y. E.; McCall, W.; Fei, X.; Liu, Y.; Ponguta, L. A.; French, F. S.; Wilson, E. M.; Earp, H. S., 3rd. Heregulin-induced activation of HER2 and HER3 increases androgen receptor transactivation and CWR-R1 human recurrent prostate cancer cell growth. *Clin. Cancer Res.* **2005**, *11* (5), 1704–12.

(20) Vogel, C. L.; Cobleigh, M. A.; Tripathy, D.; Gutheil, J. C.; Harris, L. N.; Fehrenbacher, L.; Slamon, D. J.; Murphy, M.; Novotny, W. F.; Burchmore, M.; Shak, S.; Stewart, S. J.; Press, M. Efficacy and safety of trastuzumab as a single agent in first-line treatment of HER2-overexpressing metastatic breast cancer. *J. Clin. Oncol.* **2002**, *20* (3), 719–26.

(21) Kute, T.; Lack, C. M.; Willingham, M.; Bishwokama, B.; Williams, H.; Barrett, K.; Mitchell, T.; Vaughn, J. P. Development of Herceptin resistance in breast cancer cells. *Cytometry A* **2004**, *57* (2), 86–93.

(22) Medina-Kauwe, L. K.; Kasahara, N.; Kedes, L. 3PO, a novel non-viral gene delivery system using engineered Ad5 penton proteins. *Gene Ther.* **2001**, *8*, 795–803.

(23) Medina-Kauwe, L. K.; Maguire, M.; Kasahara, N.; Kedes, L. Non-viral gene delivery to human breast cancer cells by targeted Ad5 penton proteins. *Gene Ther.* **2001**, *8*, 1753–1761.

(24) Zochowski, M.; Wachowiak, M.; Falk, C. X.; Cohen, L. B.; Lam, Y. W.; Antic, S.; Zecevic, D. Imaging membrane potential with voltage-sensitive dyes. *Biol. Bull.* **2000**, *198* (1), 1–21.

(25) Dall'Asta, V.; Gatti, R.; Orlandini, G.; Rossi, P. A.; Rotoli, B. M.; Sala, R.; Bussolati, O.; Gazzola, G. C. Membrane potential changes visualized in complete growth media through confocal laser scanning microscopy of bis-oxonol-loaded cells. *Exp. Cell Res.* **1997**, *231* (2), 260–8.

(26) Rentsendorj, A.; Xie, J.; MacVeigh, M.; Agadjanian, H.; Bass, S.; Kim, D. H.; Rossi, J.; Hamm-Alvarez, S. F.; Medina-Kauwe, L. K. Typical and atypical trafficking pathways of Ad5 penton base recombinant protein: implications for gene transfer. *Gene Ther.* **2006**, *13* (10), 821–36.

(27) Hwang, J. Y.; Lubow, J.; Chu, D.; Gross, Z.; Gray, H. B.; Farkas, D. L.; Medina-Kauwe, L. K. In *Investigating the photosensitizer-potential of targeted gallium corrole using multimode optical imaging*; SPIE Photonics West: San Francisco, CA, USA, 2011.

(28) Yamada, J.; Yoshimura, S.; Yamakawa, H.; Sawada, M.; Nakagawa, M.; Hara, S.; Kaku, Y.; Iwama, T.; Naganawa, T.; Banno, Y.; Nakashima, S.; Sakai, N. Cell permeable ROS scavengers, Tiron and Tempol, rescue PC12 cell death caused by pyrogallol or hypoxia/reoxygenation. *Neurosci. Res.* **2003**, *45* (1), 1–8.

(29) Verma, A.; Nye, J. S.; Snyder, S. H. Porphyrins are endogenous ligands for the mitochondrial (peripheral-type) benzodiazepine receptor. *Proc. Natl. Acad. Sci. U.S.A.* **1987**, *84* (8), 2256–60.

(30) Wolin, M. S. Reactive oxygen species and vascular signal transduction mechanisms. *Microcirculation* **1996**, *3* (1), 1–17.

(31) Horbinski, C.; Mojesky, C.; Kyprianou, N. Live Free or Die: Tales of Homeless (Cells) in Cancer. *Am. J. Pathol.* **2010**, *177* (3), 1044–1052.

(32) Harvey, A. J.; Pennington, C. J.; Porter, S.; Burmi, R. S.; Edwards, D. R.; Court, W.; Eccles, S. A.; Crompton, M. R. Brk protects breast cancer cells from autophagic cell death induced by loss of anchorage. *Am. J. Pathol.* **2009**, *175* (3), 1226–34.

(33) Ghavami, S.; Kerkhoff, C.; Chazin, W. J.; Kadkhoda, K.; Xiao, W.; Zuse, A.; Hashemi, M.; Eshraghi, M.; Schulze-Osthoff, K.; Klonisch, T.; Los, M. S100A8/9 induces cell death via a novel, RAGE-independent pathway that involves selective release of Smac/DIABLO and Omi/HtrA2. *Biochim. Biophys. Acta* **2008**, *1783* (2), 297–311.

(34) Hotchkiss, R. S.; Strasser, A.; McDunn, J. E.; Swanson, P. E. Cell Death. *N. Engl. J. Med.* **2009**, *361* (16), 1570–1583.

(35) Salvesen, G. S.; Duckett, C. S. IAP proteins: blocking the road to death's door. *Nat. Rev. Mol. Cell Biol.* **2002**, 3 (6), 401–410.

(36) Schafer, Z. T.; Grassian, A. R.; Song, L.; Jiang, Z.; Gerhart-Hines, Z.; Irie, H. Y.; Gao, S.; Puigserver, P.; Brugge, J. S. Antioxidant and oncogene rescue of metabolic defects caused by loss of matrix attachment. *Nature* **2009**, *461*, 109–113.